JOURNAL OF CATALYSIS 146, 375–393 (1994)

On the Structural Differences between Alumina-Supported CoMoS Type I and Alumina-, Silica-, and Carbon-Supported CoMoS Type II Phases Studied by XAFS, MES, and XPS

S. M. A. M. Bouwens,*[,1] F. B. M. van Zon,* M. P. van Dijk,† A. M. van der Kraan,‡ V. H. J. de Beer,[1] J. A. R. van Veen,*[,†] and D. C. Koningsberger*[,§,2]

*Schuit Institute of Catalysis, Eindhoven University of Technology, Postbus 513, 5600 MB Eindhoven, The Netherlands; †Koninklijke/Shell Laboratorium Amsterdam, Badhuisweg 3, 1031 CM Amsterdam, The Netherlands; ‡Interfacultair Reactor Instituut, Delft University of Technology, Mekelweg 15, 2629 JB Delft, The Netherlands; and §Laboratory of Inorganic Chemistry and Catalysis, Debye Institute, Utrecht University, P.O. Box 80083, 3508 TB Utrecht, The Netherlands

Received June 16, 1993; revised October 25, 1993

In this study the local structure of the Mo and Co promoter atoms in CoMoS type I and II on alumina, and CoMoS type II on various supports is compared using *in situ* XAFS spectroscopy as the main technique with XPS and MES in a supporting role. In the CoMoS phase the Co atoms are positioned at the edges of the MoS_2 particles, in the same plane as the Mo atoms. The CoMoS phase in all catalysts shows a well defined Co–Mo and a Mo–Co coordination. On alumina the CoMoS type II phase is present as a multilayer structure, whereas type I exists as a single-slab, i.e., monolayer, structure. The silica-supported CoMoS type II closely resembles its alumina-supported counterpart. However, the Mo–S coordination number, the structural ordering and degree of stacking of the carbon-supported type II CoMoS phase is much more similar to the type I CoMoS phase supported on alumina. This contradicts the common opinion that the CoMoS type II phase is fully sulfided and not chemically bonded to the support. Two different types of Co-sites can be distinguished in the suite of catalysts studied in this paper. A Co-site with an approximately fivefold Co–S coordination and possibly a single Co–Mo coordination is predominant in the least active alumina-supported CoMoS type I and CoMoS type II (with Co/Mo = 0.39 at/at) samples. The other Co-site has a sixfold Co–S coordination with possibly a twofold Co–Mo coordination and has the highest activity for HDS. The latter site constitutes a large part of the Co-sites in silica-supported CoMoS phase II and alumina-supported CoMoS type II (with Co/Mo = 0.32) and is exclusively present in the carbon-supported CoMoS phase II.

INTRODUCTION

Alumina-supported Co- and Ni-promoted molybdenum sulphide hydrotreating catalysts are widely used in many refineries, and research is being done continously to improve their performance. Many aspects of the preparation–structure–activity relationship have been and are being studied. The description of the active phase in these hydrotreating catalysts that has been used as a starting point for this study is due to Topsøe *et al.* (1). Their "CoMoS" model pictures the active phase as consisting of small MoS_2 particles with Co promoter atoms decorating their edges. The amount of Co in CoMoS could be determined by *in situ* ^{57}Co Mössbauer emission spectroscopy (MES) (2), and the thiophene hydrodesulphurization (HDS) activity was found to be proportional to the quantity. However, the precise local structure of the Co promoter sites is still under discussion (3). For instance, Candia *et al.* distinguished two types of CoMoS phases (type I and type II) in their study of sulphided CoMo/Al_2O_3 catalysts (4). The intrinsic thiophene HDS activity (i.e., the activity per Co in CoMoS) is much higher for type II than for type I CoMoS. Type I CoMoS is obtained by sulphidation at standard conditions (i.e., at temperatures around 673 K, atmospheric pressure using 10% H_2S in H_2) and is supposed to be bonded to the alumina support by a few Mo–O–Al linkages. Type II, which can be obtained by sulphiding at high temperatures (873 K) (4), corresponds to the fully sulphided phase, having only a weak (van der Waals) interaction with the alumina support.

As we reported recently, pure type II CoMoS can be generated, at standard sulphiding conditions, by taking the CoMo(NTA) complex (NTA = nitrilo triacetic acid) as the precursor to the active phase (5). The intrinsic thiophene HDS activities of silica- and alumina-supported type II CoMoS were found to be similar, while that of their carbon-supported counterpart was appreciably higher (5). It is clear, therefore, that the intrinsic activity of the

[1] Present address: Dow Chemical, H. Dowweg 5, 4542 NM Terneuzen, The Netherlands.

[2] To whom correspondence should be addressed.

0021-9517/94 $6.00

CoMoS phase is quite variable. On the contrary, the Mössbauer spectrum of Co in CoMoS does not appear to vary significantly upon going from one modification to the next (5, 6). A second complication has arisen recently, because the work of Van der Kraan *et al.* shows that the CoMoS Mössbauer signature is not unique: it can even be found in certain Co/C catalysts as well (7). However, there is still convincing experimental evidence from an IR study of the adsorption of NO molecules on a series of sulphided $CoMo/Al_2O_3$ catalysts that the Co atoms in the CoMoS phase are in fact associated with the MoS_2. It was found that upon increasing the Co loading at fixed Mo loading the spectrum of NO adsorbed on Co sites increased in intensity, while that of NO adsorbed on Mo sites decreased in intensity (8).

The question that remains to be answered, is whether or not the differences in catalytic activity between Al_2O_3-supported CoMoS type I and CoMoS type II, and between CoMoS type II supported on Al_2O_3, SiO_2, or carbon can be related to subtle differences in the structure of the CoMoS phase. *In situ* XAFS spectroscopy was first applied in the structural study of hydrotreating catalysts by Topsøe *et al.* (9), and subsequently also by others (10–15). Since conventionally prepared $CoMo/Al_2O_3$ catalysts contain mainly CoMoS type I after standard sulphidation (cf. Ref. (6)), a Mo–O contribution in the Mo EXAFS spectrum of such catalysts might be expected. Only Bauer *et al.* (14) have reported such a contribution, but the spectra were not obtained under strictly *in situ* conditions. Also the expected Co(Ni)–Mo contribution at about 3 Å was not found in (9, 11–15). Only Bommannavar and Montano (10) reported a Ni–Mo contribution in the Ni EXAFS spectrum of sulphided $NiMo/Al_2O_3$, while the corresponding Mo–Ni contribution in the Mo EXAFS could not be detected. However, in our recent work on a carbon-supported NiMo catalyst prepared via the NTA method, both the Ni–Mo and the Mo–Ni contributions were unequivocally present (16). A clear Co–Mo contribution was present in the Co EXAFS of CoMo(NTA)/C, but not in the conventionally prepared CoMo/C (17). From these results it is clear that considerable progress has been made in the determination of the basic structure of the CoMoS phase. However, not much information is available as to the dependence of the structural details on the preparation route and the type of support.

The object of this study is to compare the local structures of the Mo, and Co promoter atoms in CoMoS type I and II on alumina, and in CoMoS type II on various supports. *In situ* XAFS spectroscopy, with XPS and MES in a supporting role, has been applied to compare the local structures and to try to correlate any differences found to the observed differences in thiophene HDS activity.

EXPERIMENTAL

Catalyst Preparation

As support materials we employed KC310 γ-alumina (250 m^2/g), Shell silica spheres (265 m^2/g), and Norit RX3 Extra activated carbon (1200 m^2/g). The chemicals making up the impregnation solutions were at least 99% pure.

The alumina-supported CoMoS type I precursor catalyst was prepared by pore-volume impregnation of the alumina support with a clear and stable ammoniacal solution of ammonium heptamolybdate and cobalt nitrate. It contains 2.8 wt% Co and 8.2 wt% Mo in the calcined state (calcination temperature around 723 K, rather low in order to prevent the formation of a Co aluminate). On the basis of previous MES (Mössbauer Emission Spectroscopy) and thiophene HDS work (6), this catalyst can be expected to contain virtually 100% CoMoS type I upon sulphidation. It is designated CoMoS(I)/Al.

The alumina-, silica-, and carbon-supported CoMoS type II precursor catalysts were prepared via pore-volume impregnation using aqueous solutions containing the amounts of cobalt nitrate and molybdenum oxide required (Al_2O_3, C: 1.5 wt% Co and 7.7 wt% Mo; SiO_2: 1.9 wt% Co and 10.5 wt% Mo) and nitrilotriacetic acid (NTA) with NTA/Mo = 1.2 mol/mol (5). The role of NTA is to complex both Co and Mo, so that the sulphiding behaviour of the (noncalcined) catalysts is determined by the CoMo(NTA) complex rather than by a CoMo–support interaction. By using this preparation method it can be expected that regardless of the support the same CoMoS type II phase will be formed. MES showed that the NTA route using the employed Co/Mo ratio of about 0.32 at/at leads to all Co ending up in the CoMoS phase (5, 6). In the following, these catalysts will be called CoMoS(II)/Al(0.32), CoMoS(II)/Si, and CoMoS(II)/C, respectively. A second alumina-supported catalyst was prepared via the NTA-route, containing 1.8 wt% Co and 7.7 wt% Mo (Co/Mo = 0.39 at/at). This catalyst will be designated CoMoS(II)/Al(0.39).

For comparative purposes, a Co-free Mo/Al_2O_3 catalyst was prepared via pore-volume impregnation with an aqueous solution of ammonium heptamolybdate, followed by drying in air at 383 K (16 h) and calcining in air at 823 K (2 h). Its loading amounts to 8.1 wt% Mo, and it will be called Mo/Al.

Mössbauer Spectroscopy

The setup used for obtaining *in situ* Mössbauer spectra has been described previously (6). Sulphidation was carried out in a 50 cm^3/min flow of 10 mol% H_2S in H_2 gas mixture. After flushing the reactor with this gas mixture at room temperature for 30 minutes, the temperature was linearly increased at 2 K/min to 673 K, and kept there

for 1 h. Subsequent cooling was effected in argon, and the spectra were taken at room temperature.

Catalytic Activity Measurements

Catalytic activity for thiophene HDS was determined using a microflow reactor operating at 673 K and atmospheric pressure. Catalyst samples (0.2 g) were sulphided in situ in a mixture of 10 mol% H_2S in H_2 at a flow rate of 50 cm^3/min. The following temperature programme was applied: starting at 293 K, the temperature was linearly increased at 2 K/min (CoMoS type II catalysts) or 5 K/min (CoMoS(I)/Al, Mo/Al) to 673 K, and held there for 1 or 2 h, respectively. After sulphidation, the reaction mixture (consisting of 6.2 mol% thiophene in H_2) was introduced, the flow rate remaining 50 cm^3/min. The reaction products were analyzed by on-line chromatography. The concentrations measured after a 2 h run were used to calculate the first-order rate constant for HDS (17).

XPS Measurements

XPS spectra of the sulphided catalysts were recorded on an AEI ES 200 spectrometer with Al anode (1486.6 eV) and a spherical analyser operating at a pass energy of 60 eV. In order to avoid contact of the sulphided catalysts with air, a special sulphiding reactor was used (18) which allowed transfer of the samples to a N_2-flushed glove box attached to the XPS apparatus without exposure to air. After they were sulphided, under the same conditions as described above for the HDS measurements, the catalyst samples were flushed with purified He for 30 min at 673 K and subsequently cooled to room temperature. Samples were mounted on the specimen holder by means of double-sided adhesive tape. Spectra were recorded at 293 K in steps of 0.1 eV, and at a pressure lower than 1.3×10^{-6} Pa.

The C 1*s* peak (284.6 eV) was used as an internal standard for binding energy calibration. Curves were integrated applying a linear baseline. The Mo(3*d*)/Al(2*s*) (or Mo(3*d*)/C(1*s*) for the CoMoS(II)/C catalyst) photoelectron intensity ratios were used to measure the degree of dispersion of the molybdenum sulphide phase on the alumina or carbon support. Theoretical intensity ratios were calculated according to the quantitative XPS model described by Kuipers (19). Further details on the quantitative XPS analysis are given in (17).

XAFS Spectroscopy

Data collection. Spectra were recorded at the Wiggler station 9.2 at the Synchrotron Radiation Source (SRS) in Daresbury (UK). The storage ring was operated with an electron energy of 2 GeV and a current between 120 and 250 mA. The Si(220) double crystal monochromator was detuned to 50% intensity to avoid the effects of higher harmonics present in the X-ray beam. The measurements were done in the transmission mode. To decrease low- and high-frequency noise as much as possible, each data point was counted for 1 s and several scans were averaged. The oxidic samples were pressed into self-supporting wafers (the CoMo/C catalyst requires the use of a special carbon binder (17)) which were mounted in a transmission EXAFS *in situ* cell (20). Sulphidation was carried out under the same conditions as described above for the thiophene HDS test. After sulphiding, the samples were purged in purified He for 15 min at 673 K, and subsequently cooled to room temperature in flowing helium. The X-ray absorption spectra of the Co and Mo *K*-edges were recorded in a static He atmosphere at liquid nitrogen temperature. A few exceptions occurred to the above procedures: in the case of the Mo *K*-edge EXAFS measurements of the CoMoS(II)/Si and CoMoS(II)/C catalysts, the final sulphidation temperatures were 643 and 623 K, respectively. In the latter measurement, moreover, the sample was cooled in a flow of the sulphiding gas mixture down to 373 K, and only thereafter in a flow of He to room temperature, and the Mo *K*-edge absorption spectrum was also recorded at this temperature.

Data reduction. Standard procedures were used to extract the EXAFS data from the measured absorption spectra (21, 22). Normalization was done by dividing the absorption intensities by the height of the absorption edge and subtracting the background using cubic spline routines. The final EXAFS function was obtained by averaging the individual background-subtracted and normalized EXAFS data. The standard deviations were calculated for the individual EXAFS data points as a measure of the random error in the final EXAFS function. The EXAFS data analysis is usually performed on an isolated part of the data obtained by an inverse Fourier transformation over a selected range in *r*-space. The isolated EXAFS function was obtained by averaging the inverse Fourier transformations of each individual EXAFS data set. The standard deviation calculated from the individual data points of the several isolated EXAFS functions provided a measure of the random error in the average isolated EXAFS function.

Reference data. Data for the phase shifts and backscattering amplitudes were obtained from EXAFS measurements of reference compounds. For the Co–S EXAFS signals CoS_2 was used, for the Co–Co contributions the Ni–Ni coordination in NiO was chosen, and for the Mo–S and Mo–Mo EXAFS functions, the respective first-shell coordinations of MoS_2 were employed. Finally, for the Co–Mo and Mo–Co contributions in the promoted catalysts we took $((C_6H_5)_4P)_2Ni(MoS_4)_2$ as the reference compound. The use of a Ni absorber or backscatterer instead of Co appears to be justified in the light of Teo and Lee's work (23).

NiO was obtained from Merck (p.a.) and MoS_2 from Janssen Pharmaceutica (min.99%), CoS_2 was prepared according to Morris's recipe (24), while the Ni–Mo cluster compound was prepared by Baumann (Un. Bielefeld, FRG).

The production of the Co–S, Co–Co (Ni–Ni), and Co–Mo (Ni–Mo) EXAFS references is described in (17) and of the Mo–S, Mo–Co (Mo–Ni), and Mo–Mo references in (25).

Data analysis. The spectra have been analyzed using an improved version of the Eindhoven EXAFS data analysis software (NEX), now including statistical analysis. The statistical analysis is based upon the methods described in the *Report on Standards and Criteria in XAFS Spectroscopy* (27). The parameters extracted from the measurements are coordinated number N, coordination distance R, and Debye–Waller factor $\Delta\sigma^2$ and inner potential ΔE_0 (both with respect to the appropriate reference compound) for the various coordination shells. Previously, a comparison of the analysis results from the EXCURVE (28) and our own package showed that the parameters extracted for the dominant coordination shell are very similar, but some differences develop for the less prominent shells (29). Recently, however, it was shown (30) that the systematic errors produced by Fourier filtering (used to obtain phase shifts and backscattering amplitudes from reference compounds) are much smaller than the systematic errors introduced by the use of theoretical references. Therefore, experimental references have been used in this study to further investigate the catalytic samples. Moreover, it is now possible for us to calculate the standard deviations in the coordination parameters including the actual noise in the data. To reliably determine the parameters characterizing the high-Z (Mo) and low-Z (S, Co) contributions, multiple-shell fitting in k-space and in r-space was done with application of both k^1 and k^3 weighting. This ensures a better decoupling of the EXAFS parameters (R vs ΔE_0 and N vs $\Delta\sigma^2$) than could be realized if only k^1 or k^3 weighting was applied in the fitting (31). The different contributions present in the spectra were identified by applying the difference file technique and phase- and amplitude-corrected Fourier transforms (22, 31). In order to determine whether not only the dominant contribution(s) but also an extra (smaller) contribution can be extracted reliably from the EXAFS spectra, the so-called F-test was applied. In this test, well-known in the field of statistics, residuals of a fit with or without the small contribution are compared, and a statistical probability of the existence of such a small contribution is calculated (27).

RESULTS

Catalytic Properties

The thiophene HDS reaction rate constants, k_{HDS}, per mol Co, of the promoted catalysts are shown in Fig. 1.

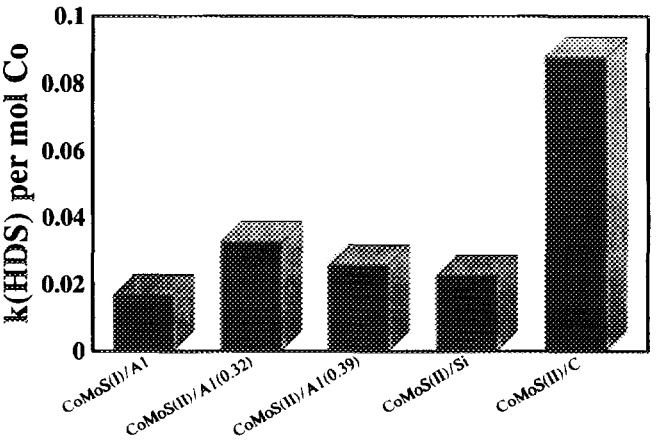

FIG. 1. Thiophene HDS reaction rate constants, k_{HDS}, per mol Co present, of the sulfided CoMoS(I)/Al, CoMoS(II)/Al(0.32), CoMoS(II)/Al(0.39), CoMoS(II)/Si, and CoMoS(II)/C catalysts.

Since in all catalysts Co is present in a CoMoS phase, the values reported in Fig. 1 can be regarded as being the specific activities per mol Co in CoMoS. It follows that the specific activity of the CoMoS(II)/Al(0.32) catalyst is twice as high as that of the conventionally prepared CoMoS(I)/Al catalyst, which is in accordance with the data of alumina-supported CoMoS type I and II reported by Candia *et al.* (4). The specific activity of CoMoS(II)/Al(0.39) is significantly lower than that of CoMoS(II)/Al(0.32) (the activities per g catalyst are equal). This is remarkable, since CoMoS(II)/Al(0.32) and CoMoS(II)/Al(0.39) give very similar MES spectra (Fig. 2) with no significant differences in the derived Mössbauer promoters (IS, QS). It can therefore be concluded that in both cases virtually all Co ends up in the CoMoS phase. The

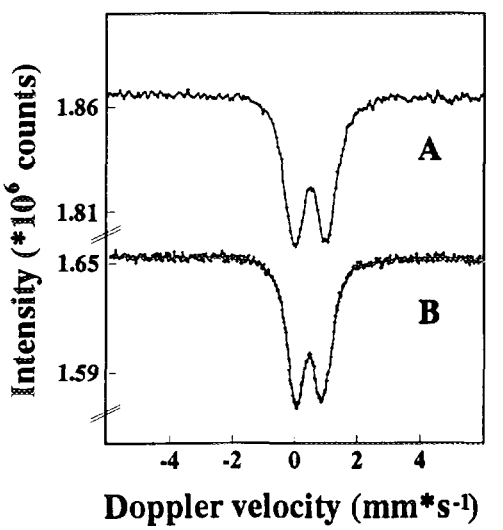

FIG. 2. In situ Mössbauer Emission spectra of (A) sulfided CoMoS(II)/Al(0.32) and (B) CoMoS(II)/Al(0.39).

TABLE 1

XPS Results of the Sulphided Catalysts

	Mo/Al	CoMoS(I)/Al	CoMoS(II)/Al(0.32)	CoMoS(II)/C
XPS binding energies (eV)				
Co $2p_{3/2}$		778.6	778.6	778.6
S $2p$	162.7	161.9	161.2	162.5
ΔE_1 (Co $2p_{3/2}$ − S $2p$)		616.7	617.4	616.1
Mo $3d_{5/2}$	229.8	228.6	228.1	229.1
ΔE_2 (Mo $3d_{5/2}$ − S $2p$)	67.1	66.7	66.9	66.6
Quantitative results				
$(I_{Mo}/I_{Al})_{exp}$	0.7	1.2	0.4	0.1[a]
$(I_{Mo}/I_{Al})_{theor}$	0.9	1.0	0.9	0.1[a]
MoS_2 particle thickness (nm)	0.6	0.3	3.0	0.5
$(I_{Co}/I_{Al})_{exp}$		1.1	0.3	0.14[b]
S/(Co + Mo) (mol/mol)	1.4	1.4	1.5	2.1

Note. $(I_{Mo}/I_{Al})_{theor}$ is the intensity ratio for the case of a monolayer dispersion. Accuracies for the XPS binding energies ±0.2 eV; for $(I_{Mo}/I_{Al})_{exp}$ ± 25%; for $(I_{Co}/I_{Al})_{exp}$ ± 30%; for S/(Co + Mo) ± 15%.

[a] I_{Mo}/I_C.

[b] I_{Co}/I_C.

specific activity of CoMoS(II)/Si is also lower than that of CoMoS(II)/Al(0.32), which is inconsistent with our previous work (5). We have traced this to an ageing effect, the CoMoS(II)/Si catalyst being the one material that was not freshly prepared for this study: the sample employed was about one year old, and apparently the CoMo(NTA) complex slowly decomposes over time. A thiophene HDS test on a freshly prepared sample gave the expected result (5): a specific activity about equal to that of CoMoS(II)/Al(0.32) (N.B. the catalytic properties and EXAFS results for CoMoS(II)/Si presented here have been obtained from samples of similar age). The specific activity of Co MoS(II)/C is considerably higher than that of the other catalysts (Fig. 1), in agreement with our previous work (5). As far as the Mo/Al catalyst is concerned, its k_{HDS} of 0.6×10^{-3} m^3/kg/s is much lower than the corresponding value of 6.9×10^{-3} m^3/kg/s for the CoMoS(I)/Al catalyst.

XPS Measurements

The XPS characteristics of the sulphided catalysts are collected in Table 1. As was outlined by Alstrup *et al.* (32), a reliable way to compare XPS binding energies (BE) from different samples is to use energy differences. Hence, Table 1 shows two BE differences, ΔE_1 and ΔE_2, obtained by substracting the BE of the S $2p$ peak from that of the Co $2p$(3/2) peak and from that of the Mo $3d$ (5/2) peak, respectively. The values of ΔE_1 for CoMoS(I)/Al, 616.7 eV, and CoMoS(II)/Al(0.32), 617.4 eV, are reasonably close to the value of 617.0 eV which, according to Alstrup *et al.*, is characteristic of Co in the CoMoS phase. On the other hand, ΔE_1 for the CoMoS(II)/C sample, 616.1 eV, would be typical for Co_9S_8 (32), a conclusion that is flatly contradicted by the MES results which unequivocally show that Co is only present in a CoMoS phase. Whether or not this is indicative of a strong CoMo S(II)–carbon interaction, it can be concluded that our XPS data are not a reliable guide to the phase composition of a sulphided CoMo catalyst. The values of ΔE_2, 66.6–67.1 eV, correspond closely to the value of 66.9 eV reported for pure MoS_2 by Alstrup *et al.* (32).

The quantitative XPS intensity results reveal significant differences between the catalysts. For the Mo/Al and CoMoS(I)/Al catalysts the experimental Mo/Al intensity ratios are reasonably close to the theoretical value for a monolayer dispersion. For Mo/Al a MoS_2 particle thickness of about 0.6 nm was calculated, which is about the crystallographic thickness of a MoS_2 single slab (0.615 nm (33)). For CoMoS(I)/Al the experimental Mo/Al intensity ratio comes out at a somewhat higher value, 1.2, than the theoretical maximum, 0.96. Since the experimental accuracy is ±25%, we conclude that the CoMoS(I) phase is at maximum dispersion, which probably means that it exists as extremely small single-slab particles on the alumina surface. The Mo/Al intensity ratio of the CoMo S(II)/Al(0.32) catalyst is quite low (0.4) as compared to that of the above two materials. A MoS_2 particle thickness of 3.0 nm was calculated, which suggests the presence of multilayers of MoS_2 slabs. In contrast, for the CoMoS(II)/C catalyst a particle thickness of 0.5 nm was calculated, which is consistent with a monolayer dispersion of MoS_2.

As far as the Co/Al intensity ratio is concerned, it appears that in the CoMoS(I)/Al catalyst this ratio is about four times higher than in CoMoS(II)/Al(0.32), 1.1 vs 0.3. Correcting for the Co loading of the two samples (2.8 vs 1.4 wt%), the difference in Co/Al ratio reduces to a factor of 2, still highly significant and indicating that the Co atoms in CoMoS(II)/Al(0.32) are partly obscured. The

total sulphur content, expressed as the ratio S/(Co + Mo), appears to be much higher for the CoMoS(II)/C sample than for all the alumina-supported catalysts. They are very similar in this respect; the value for CoMoS(II)/Al(0.32) being only slightly higher than that for Mo/Al and CoMoS(I)/Al (Table 1).

XAFS Spectroscopy

Co EXAFS. In Fig. 3 the raw Co K-edge EXAFS spectra of the sulphided catalysts are shown. In some spectra, a feature around $k = 13$ Å^{-1} is observed (due to a small contamination of Ni); otherwise, the noise level is very low and estimated to be around 0.002. The Co–S and Co–Mo coordinations were filtered by applying a forward ($\Delta k = 2.8$–10.1 Å^{-1} for CoMoS(II)/Si and CoMoS(II)/C, $\Delta k = 2.8$–11.1 Å^{-1} for the other samples) and inverse FT ($\Delta r = 0.8$–3.2 Å). The Fourier transforms of the filtered spectra (only shown for CoMoS(II)/Al(0.32) in Fig. 4A) are dominated by a large Co–S peak, but for all samples also a smaller peak is clearly present at $R = 2.5$–3.0 Å (subsequent analysis showed that this peak should be attributed to a Co–Mo coordination). Differences in magnitude and imaginary part of the Co–S and Co–Mo peaks in the Fourier transforms of the individual samples show that, although the coordination environment for the Co atoms is similar in all samples, the exact number and arrangement of S and Mo neighbours varies depending on the support and preparation method used.

The filtered EXAFS functions were fitted using the Co–S and Co–Mo reference EXAFS functions (17). In the analysis of the CoMoS catalysts it could not be excluded that the spectra of the catalysts contain a Co–Co coordination as well. However, it was found that inclusion of an extra Co–Co shell in the fit was not statistically significant. For CoMoS(II)/Al(0.32) the filtered (solid line) and best-fit (dotted line) EXAFS functions are shown in r-space (k^1-weighted Fourier transform, Fig. 4A) and k-space (Fig. 4B). The structural parameters obtained from the EXAFS fitting routine are collected in Table 2 together with values of the goodness of fit (ε_ν^2) as defined in (27).

In order to check the appropriateness of the addition of the Co–Mo contribution (which is small when compared with the Co–S contribution), a two-shell fit, including the Co–S as well as Co–Mo contribution, was compared with the one-shell fit with only the Co–S shell present. The result of this comparison is depicted for CoMoS(II)/Al(0.32) in Fig. 4. For the one-shell fit, the k^1-weighted FT of the best fit Co-S EXAFS function together with the FT of the filtered EXAFS are shown in Fig. 4C; the k^1-weighted FT of the difference file (filtered EXAFS minus best Co–S contribution) is shown in Fig. 4D, it still contains a sizeable peak around 3 Å (a remnant of the background signal is also visible at 1–1.5 Å). Figure 4A displays the k^1-weighted FT of the best two-shell fit Co–S + Co–Mo EXAFS function together with the filtered EXAFS. The k^1-weighted FT of the difference file (filtered EXAFS minus best Co-S contribution), together with the best Co–Mo contribution, are shown in Fig. 4E, and the same functions (together with an indication of the noise level) in k-space in Fig. 4F. In k-space, minima and maxima of the difference file and best fit Co–Mo contribution are found at the same positions; only their magnitude differs because a low-frequency, residual background oscillation is also present in the difference file. Comparison of Figs. 4D and 4E shows that the residue in the one-shell fit almost exactly coincides with the peak ascribed to the Co–Mo contribution in the two-shell fit. Thus, the results clearly show the presence of a Co–Mo contribution. The number of independent parameters calculated from the Nyquist theorem (27) is 10.7, giving 6.7 degrees of freedom for the fit with only a Co–S contribution and 2.7 degrees of freedom for the fit with both a Co–S and Co–Mo contribution. Applying an F-test for including the Co–Mo shell (four extra fit parameters) leads to a confidence limit of 62% for the Co–Mo contribution in the EXAFS data. Taking into account the 62% confidence limit and the results shown in Fig. 4, we conclude that the two-shell fit gives the best description of the EXAFS data of the CoMoS samples. Therefore, only the coordination parameters obtained in the two-shell fits are presented.

From Table 2 it is clear that indeed the environment of the Co atoms (S, Mo atoms) in the various catalysts is rather similar. With respect to the Co–Mo contribution it is suspected that the variation in Co–Mo coordination distance has a physical origin.

Co XANES. In two recent papers (17, 34), we reported on the Co $1s$ to $3d$ transition which is present as a weak pre-edge absorption peak. This transition should provide information about the local Co site symmetry, as was demonstrated by Shulman *et al.* (35). A high intensity of the $1s$–$3d$ peak is indicative of sites lacking a symmetry centre (tetrahedral or square-pyramidal), whereas a low intensity points to sites containing a centre of inversion or a symmetry plane (octahedral, square-planar or trigonal prismatic). Inspection of the XANES for the catalyst samples, collected in Fig. 5, shows small differences in local structure for Co: the pre-edge feature (indicated by an arrow in Fig. 5A) is faint, indicating an inclination towards octahedral or perhaps trigonal prismatic coordination of S around Co. The relatively best resolved pre-edge peak is seen for the samples CoMoS(I)/Al and CoMoS(II)/Al(0.39). The intensity, however, is by far not as high as in the spectrum of CoS/C (34), in which small Co_9S_8-like

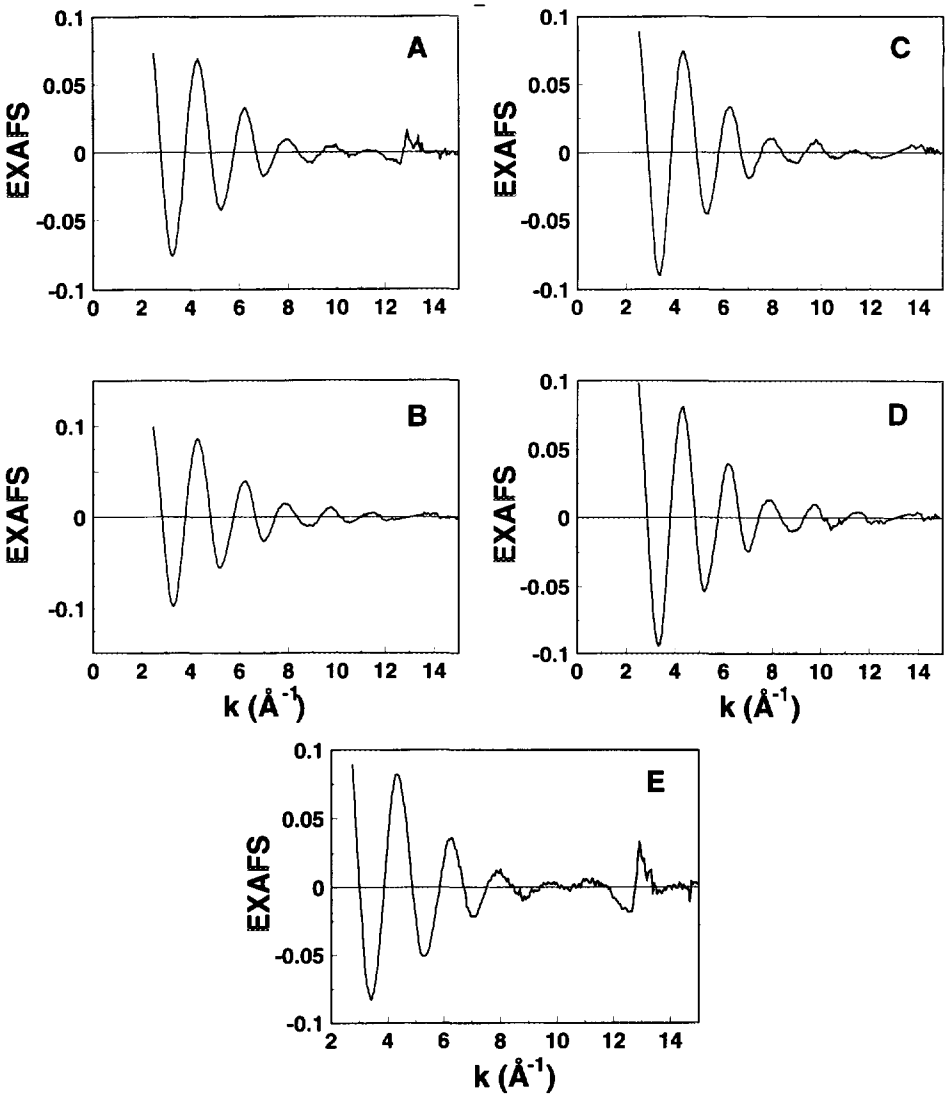

FIG. 3. Co *K*-edge raw EXAFS data of the sulfided (A) CoMoS(I)/Al, (B) CoMoS(II)/Al(0.32), (C) CoMoS(II)/Al(0.39), (D) CoMoS(II)/Si, and (E) CoMoS(II)/C.

particles were shown to be present (17), where eight out of nine Co atoms are tetrahedrally coordinated. Although the intensity of the pre-edge feature is small for the different catalysts there seems to be a correlation with the Co–S coordination, the intensity being highest for CoMoS(I)/Al with $N_{\text{co-S}} = 4.9$ and smallest for CoMoS(II)/C with $N_{\text{Co-S}} = 6.3$. Other differing features, e.g., the form of the top of the edge, are also observed in Fig. 5. However, in this region the spectra are very much influenced by multiple scattering effects, indicative of long-range order which is not the scope of this article.

Mo EXAFS. In Fig. 6 the raw Mo *K*-edge EXAFS functions of the sulphided catalysts are shown including that of the Mo/Al sample (Fig. 6A). The estimated noise in the spectra is 0.0004. As in the case of the Co-edge measurements, it is clear again that the environment of the Mo-atoms in all samples does not differ greatly. Peaks that are attributed to Mo–S (around 2 Å) and Mo–Mo (around 3 Å) coordinations are present in all spectra (shown only for CoMoS(II)/Al(0.32) in Fig. 7A). For CoMoS(II)/C it is observed that the magnitude of the peaks is smaller than for the other samples. This sample was measured at room temperature, which may at least partly account for the observed effect. A small but significant difference can be observed between the Fourier transform of the Mo/Al EXAFS data and the Fourier transforms of all the other data. For Mo/Al, the separation

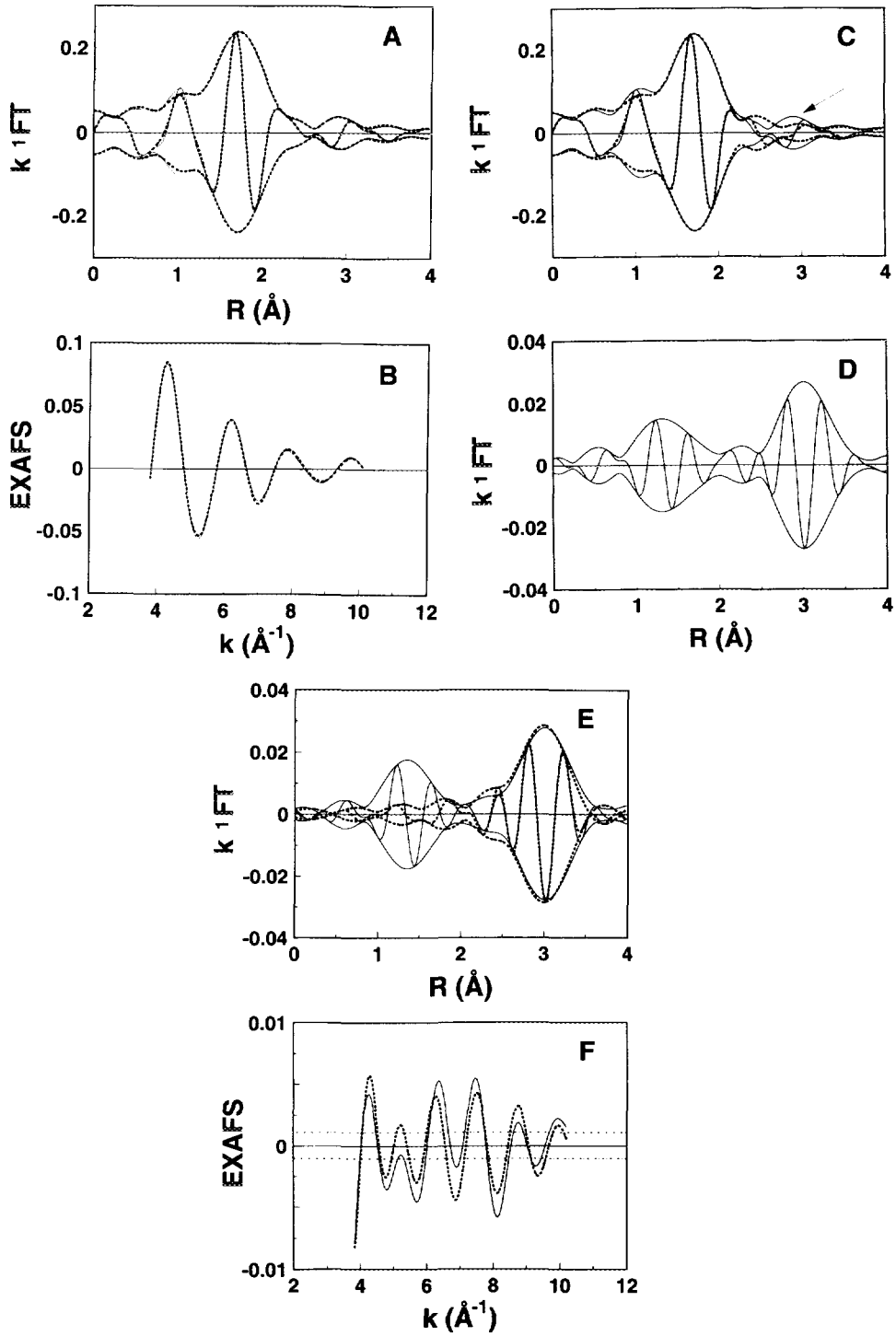

FIG. 4. Results for the Co K-edge data of CoMoS(II)/Al(0.32). (A) k^1-weighted Fourier transform (Δk = 3.8–10.2 Å^{-1}) of isolated EXAFS data (solid line) and sum of best Co–S + Co–Mo contributions (two-shell fit) (dotted line); (B) isolated EXAFS data (solid line) and best two-shell fit (dotted line) in k space; (C) k^1-weighted Fourier transform (Δk = 3.8–10.2 Å^{-1}) of isolated EXAFS data (solid line) and best Co–S contribution (one-shell fit) (dotted line) of (D) isolated EXAFS data minus best Co–S contribution (one-shell fit) of (E) isolated EXAFS data minus best Co–S contribution (two-shell fit) (solid line) and best fit Co–Mo contribution (dotted line). (F) Isolated EXAFS data minus best fit Co–S EXAFS contribution (two-shell fit) (solid line) and best fit Co–Mo EXAFS contribution (dotted line). In (F) the noise level is indicated by a dashed line.

TABLE 2

Coordination Parameters Derived from the Co-Edge EXAFS Data

Parameters	N	$\Delta(N)$	$\Delta\sigma^2$ ($\times 10^3$)	$\Delta(\Delta\sigma^2)$ (Å^2)	R (Å)	$\Delta(R)$	ΔE_0 (eV)	$\Delta(\Delta E_0)$	ε_ν^2
$CoMoS(I)/Al_2O_3$ (0.56)									1.21
Co–S	4.9	0.1	1.8	0.3	2.204	0.002	5.8	0.3	
Co–Mo	1.0	0.3	5.7	2.8	2.81	0.01	−1.0	1.5	
$CoMoS(II)/Al_2O_3$ (0.32)									1.39
Co–S	5.6	0.1	−0.4	0.3	2.216	0.002	5.0	0.3	
Co–Mo	1.5	0.3	5.3	1.8	2.87	0.01	−11.3	1.1	
$CoMoS(II)/Al_2O_3$ (0.39)									0.86
Co–S	5.2	0.2	1.1	0.5	2.217	0.003	3.2	0.4	
Co–Mo	0.9	0.4	3.9	4.0	2.86	0.02	−7.8	2.3	
CoMoS(II)/Si (0.30)									2.78
Co–S	5.4	0.1	−0.2	0.4	2.212	0.003	5.2	0.4	
Co–Mo	1.4	0.3	4.1	2.3	2.89	0.01	−13.6	1.3	
CoMoS(II)/C (0.32)									2.08
Co–S	6.3	0.2	3.0	0.4	2.212	0.003	2.9	0.4	
Co–Mo	1.9	0.5	9.2	3.0	2.82	0.02	−6.5	1.6	

between the Mo–S and Mo–Mo peaks is more distinct and the imaginary part of the Fourier transform around 2.3 Å is completely different in shape as compared to all the other samples.

The Mo–S and Mo–Mo coordination shells were isolated by a k^3-weighted FT (Δk = 3.1–14.1 Å^{-1}), followed by an inverse transform with Δr = 1.0–3.2 Å. The resulting EXAFS functions were first fitted introducing only a Mo–S and Mo–Mo coordination. However, in this way it was impossible to reproduce the feature around 2.3 Å, described above. Since the promoted catalysts can be expected to contain also a Mo–Co coordination shell (a Co–Mo contribution was found from the analysis of the Co EXAFS data!), an additional Mo–Co EXAFS function was included, which was found to have a coordination distance around 2.8 Å (due to the phase shift in the EXAFS data, this contribution appears at a smaller R of about 2.3 Å). In Fig. 7A the k^1-weighted Fourier transform and in Fig. 7B the EXAFS function of the filtered experimental data and best fit are shown for CoMoS(II)/Al(0.32) only.

Also in this case the inclusion of a Mo–Co contribution is justified by comparison of a two-shell fit (Mo–S and Mo–Mo) (see Fig. 7C) and a three-shell fit (Mo–S, Mo–Mo, and Mo–Co) (see Fig. 7A) for CoMoS(II)/Al(0.32). The Fourier transforms of the difference files (Figs. 7D–7F) clearly demonstrate the presence of an additional scatterer around 2.8 Å. In Fig. 7F, also the noise level is indicated. The number of independent parameters calculated from the Nyquist theorem (27) is 13.5, giving 5.5 degrees of freedom for the fit with only a Mo–S and Mo–Mo contribution and 1.5 degrees of freedom for the fit including an extra Mo–Co contribution. Applying an F-test for including the Mo–Co shell (four extra fit parameters) leads to a confidence limit of 89% for the Mo–Co contribution in the EXAFS data. The structural parameters derived for the three-shell fits only, together with the goodness of fit values (ε_ν^2) are collected in Table 3.

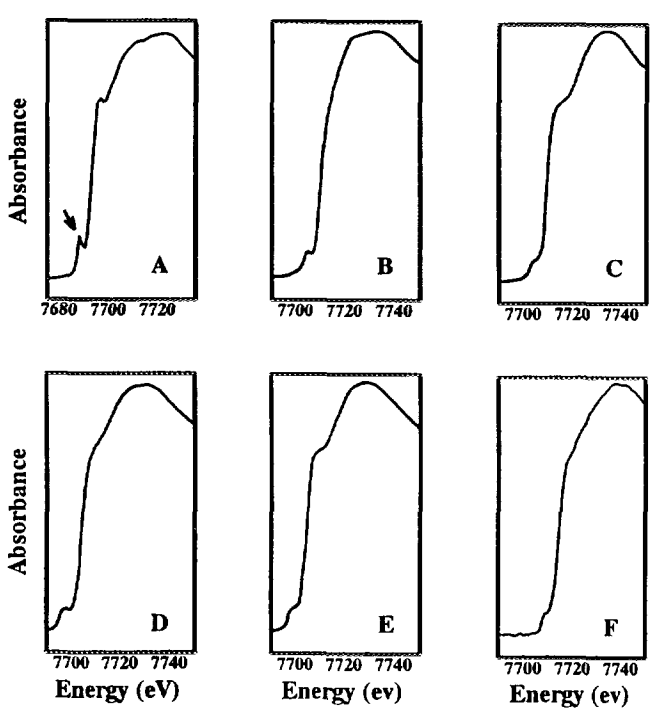

FIG. 5. Co K-edge XANES of (A) Co_9S_8, (B) CoMoS(I)/Al, (C) CoMoS(II)/Al(0.32), (D) CoMoS(II)/Al(0.39), (E) CoMoS(II)/Si, and (F) CoMoS(II)/C.

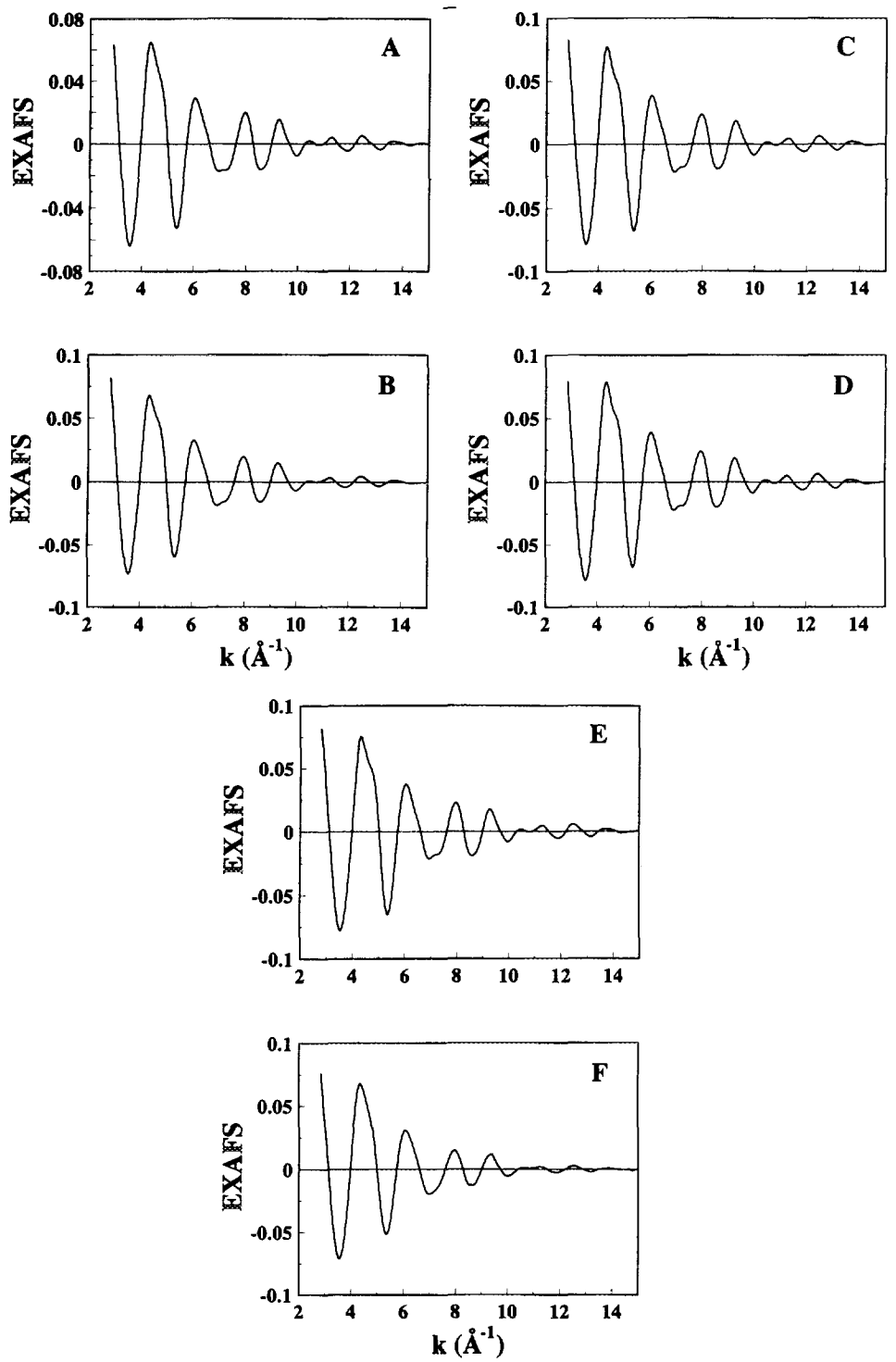

FIG. 6. Mo *K*-edge raw EXAFS data for (A) Mo/Al, (B) CoMoS(I)/Al, (C) CoMoS(II)/Al(0.32), (D) CoMoS(II)/Al(0.39), (E) CoMoS(II)/Si, and (F) CoMoS(II)/C.

DISCUSSION

This section has been divided in four parts. First, the details of the overall structures of the various CoMoS phases, as they would appear to emerge from the present XPS and the EXAFS data analysis will be discussed in "Structure of MoS_2 in the Type I and II CoMoS Phases" and "Structure around Co in Type I and II CoMoS Phases," respectively. The refined model description of the CoMoS type I and II phases will then be presented in "Structural Model." Finally, the derived structural characteristics will be related to the observed thiophene HDS activities in "Catalytic Characteristics."

Structure of MoS_2 in the Type I and II CoMoS Phases

Quantitative XPS results. The XPS results indicate that in the Al_2O_3 supported type I CoMoS catalyst the MoS_2 particles have a monolayer dispersion (one slab thick), whereas in the alumina supported type II CoMoS catalyst a multilayer MoS_2 structure is present. Taking the thickness of a MoS_2 slab to be about 0.6 nm, the MoS_2 particle thickness of 3.0 nm in CoMoS(II)/Al(0.32) would imply a stack of about five slabs. Additional support for the conclusion that stacking of MoS_2 slabs occurs in CoMoS(II)/Al(0.32), but not in CoMoS(I)/Al, is provided by the Co/Al XPS intensity ratios (Table 1). The fact that the Co/Al intensity ratio is about two times higher (when normalised to the Co content) in the latter as compared to the former catalyst indicates that in the CoMoS(I)/Al sample the Co atoms are more exposed. In the case of multilayer MoS_2 stacks, a Co atom decorating the MoS_2 edges nearest to the alumina surface will be partly shadowed by the MoS_2 slabs on top, which will lead to a decreased Co/Al XPS intensity ratio. The XPS results for CoMoS(II)/C indicate that in this sample the MoS_2 slabs are present in monolayer dispersion like in CoMoS(I)/Al, although the sample had been prepared via the NTA (CoMoS(II)) route.

The conclusions from XPS are consistent with HREM studies by Candia *et al.* (4). A $CoMo/Al_2O_3$ catalyst exhibits a transformation from a type I to type II CoMoS phase upon increasing the sulphiding temperature. Stacking of MoS_2 slabs could be clearly observed, while this could not be seen in the type I CoMoS phase obtained after low-temperature sulphiding. Clear evidence for the occurrence of MoS_2 multilayers was also recently reported by Kemp *et al.* (36), who studied alumina-supported NiMoS and CoMoS catalysts with HRTEM. They found that conventionally prepared CoMoS catalysts contained after low temperature sulphidation MoS_2 primarily as monolayers, whereas impregnation with a phosphoric-acid solution resulted in stacking of the MoS_2 layers. This is nicely in agreement with the idea elaborated elsewhere, that the presence of phosphorus induces the formation of some phase II CoMoS (6, 37).

Mo EXAFS results. No direct evidence for mono/multilayer arrangement has been found, viz., no different types of neighbouring atoms are detected for CoMoS(I) vs CoMoS(II). In the monolayer arrangement, one may expect some evidence of Mo–support linkages that help stabilize the monolayer structure (Co–support linkages could occur as well). For the multilayer MoS_2 stacks, ordering of the stack might result in higher Mo–Mo and Mo–S coordination shells arising from intra- as opposed to interslab coordinations. Differences in the EXAFS parameters of the various samples, which may fit with the model of type I CoMoS phase being a monolayer and type II phase being a multilayer structure (on alumina and silica) will be discussed below.

The Mo EXAFS data of the catalysts (Table 3) reveal an increase in the Mo-S coordination number in the order Mo/Al < CoMoS(I)/Al, CoMoS(II)/C < CoMoS(II)/Si, CoMoS(II)/Al. This indicates (i) that the Mo atoms become more sulphided in the presence of Co atoms, and (ii) that the degree of sulphiding is highest for the type II CoMoS phase. The first observation is in line with the work of Boudart *et al.* (38), who showed that in sulphided $CoMo/Al_2O_3$ catalysts the number of sulphur first neighbours of Mo increases with increasing Co/(Co + Mo) atomic ratio (up to 0.33, i.e., Co/Mo = 0.5 at/at). In the CoMoS(II)/Al catalysts, the high Mo-S coordination numbers, 6.3–6.5 (Table 3), indicate that virtually all the Mo atoms are completely, i.e., sixfold, coordinated by sulphur atoms as for bulk MoS_2. This is in line with the definition of type II CoMoS (completely sulphided phase) and the chemistry of the NTA-preparation route (cf. Experimental and (5)). On the other hand, the Mo–S coordination number in CoMoS(I)Al, where some Mo–O–Al linkages are thought to remain (4), is not very much lower (6.1). There are no Mo–O–Al linkages detected in the EXAFS spectra, which would imply that if some are present only a small number of such linkages remain after sulfiding.

From Table 3 it can be seen that the Mo–S coordination number in CoMoS(II)/Si is the same as that in CoMoS(II)/Al(0.32). For CoMoS(II)/C, on the other hand, a somewhat lower Mo–S coordination number is found. (The high Debye–Waller factors for the coordination shells in CoMoS(II)/C are thought to be mainly due to the fact that this sample has been measured at room temperature.) This could be due to the lower sulphiding temperature (623 K) of this sample. However, it should be noted that full sulphidation is normally achieved at that temperature in the case of samples prepared via the NTA-route (5). The sample was cooled down in the sulphiding gas mixture, in contrast to the silica- and alumina-supported CoMoS(II)

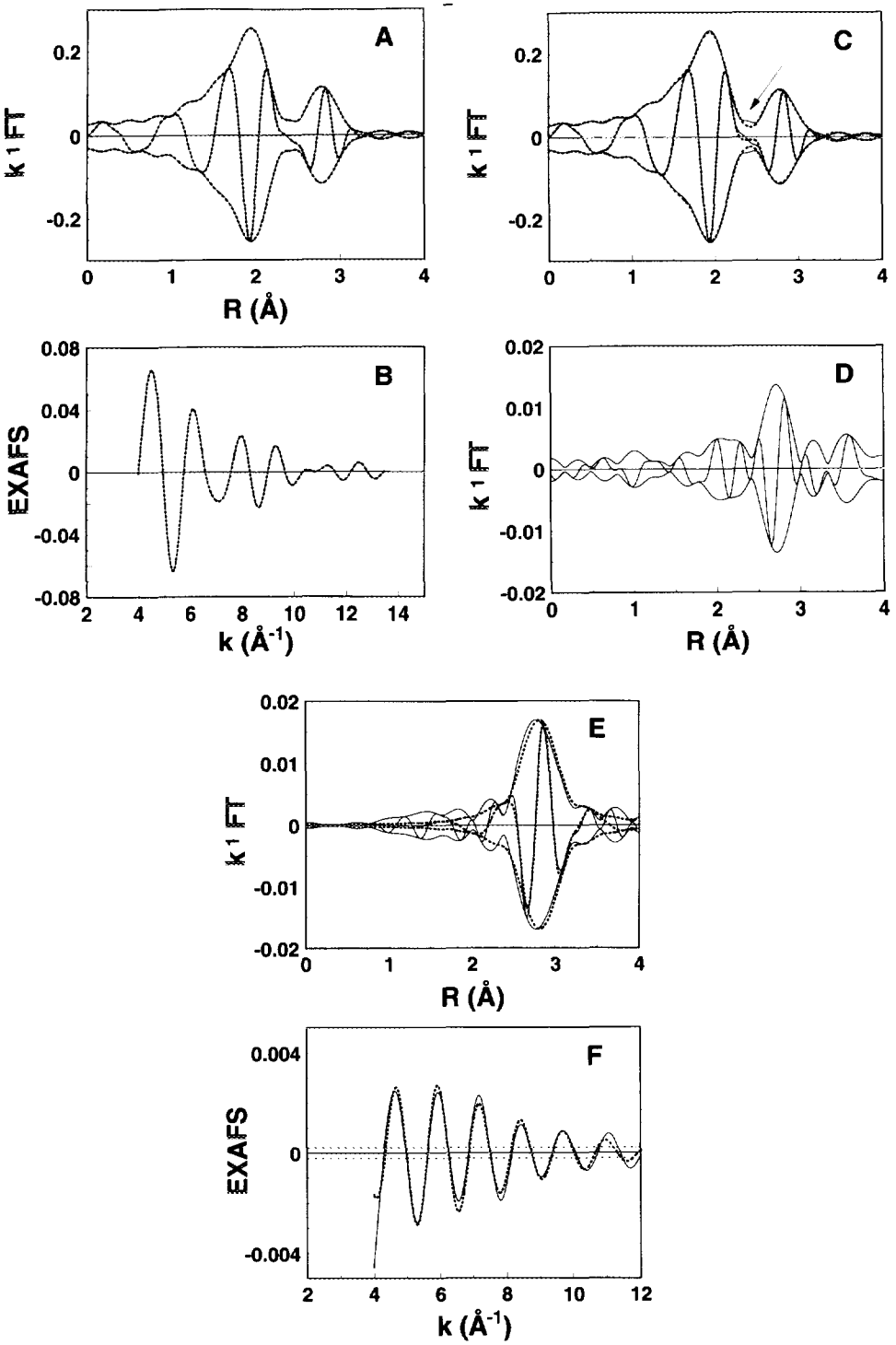

FIG. 7. Results for the Mo K-edge data of CoMoS(II)/Al(0.32). (A) k^1-weighted Fourier transform (Δk = 4.0–13.5 Å^{-1}) of isolated data (solid line) and best Mo–S + Mo–Mo + Mo–Co contributions (three-shell fit) (dotted line); (B) isolated EXAFS data (solid line) and best three-shell fit (dotted line) in k space; (C) k^1-weighted Fourier transform (Δk = 4.0–13.5 Å^{-1}) of isolated data (solid line) and best Mo–S + Mo–Mo contributions (two-shell fit) (dotted line) of (D) isolated data minus best Mo–S and Mo–Mo contributions (two-shell fit) of (E) isolated data minus best Mo–S and Mo–Mo contributions (three-shell fit) (solid line) and best Mo–Co contribution (dotted line). (F) Isolated EXAFS data minus best fit Mo–S and Mo–Mo EXAFS contributions (three-shell fit) (solid line) and best fit Mo–Co EXAFS contribution (dotted line). In (F) the noise level is indicated by a dashed line.

TABLE 3

Coordination Parameters Derived from the EXAFS Mo-Edge Data

Parameters	N	$\Delta(N)$	$\Delta\sigma^2$ ($\times 10^3$)	$\Delta(\Delta\sigma^2)$ (Å^2)	R (Å)	$\Delta(R)$	ΔE_0 (eV)	$\Delta(\Delta E_0)$	ε_ν^2
Mo/Al_2O_3									13.8
Mo–S	5.1	0.1	1.4	0.1	2.410	0.001	3.1	0.1	
Mo–Mo	3.2	0.1	2.0	0.1	3.148	0.001	4.4	0.1	
$CoMoS(I)/Al_2O_3$ (0.56)									6.55
Mo–S	6.1	0.1	2.3	0.1	2.415	0.002	1.2	0.2	
Mo–Mo	2.8	0.1	2.1	0.2	3.153	0.002	1.8	0.4	
Mo–Co	0.6	0.2	2.8	2.6	2.77	0.02	17.5	3.6	
$CoMoS(II)/Al_2O_3$ (0.32)									7.16
Mo–S	6.3	0.1	1.4	0.1	2.412	0.001	2.3	0.1	
Mo–Mo	3.3	0.3	1.2	0.3	3.150	0.003	3.3	0.6	
Mo–Co	0.7	0.3	3.4	4.0	2.83	0.02	3.4	1.9	
$CoMoS(II)/Al_2O_3$ (0.39)									4.52
Mo–S	6.5	0.1	1.6	0.1	2.415	0.001	1.8	0.1	
Mo–Mo	3.4	0.2	1.3	0.3	3.155	0.003	2.9	0.4	
Mo–Co	0.6	0.2	1.2	2.8	2.82	0.02	5.7	1.8	
CoMoS(II)/Si (0.30)									4.96
Mo–S	6.3	0.1	1.7	0.1	2.413	0.001	2.0	0.1	
Mo–Mo	3.1	0.3	1.3	0.3	3.155	0.004	2.5	0.6	
Mo–Co	0.6	0.3	3.4	4.3	2.84	0.03	3.5	2.4	
CoMoS(II)/C (0.32)									13.6
Mo–S	6.1	0.1	3.3	0.2	2.409	0.002	2.8	0.3	
Mo–Mo	2.3	0.2	3.6	0.4	3.138	0.004	3.9	0.7	
Mo–Co	0.7	0.3	6.5	4.3	2.78	0.04	18.2	5.8	

catalysts, which would tend to lead to a higher Mo–S coordination number (H_2S adsorption). EXAFS measurements on a NiMoS(II)/C sample, similar to the one reported in (16), and pretreated in the standard way, revealed a Mo–S coordination number close to that in CoMoS(I)/Al, in full agreement with the CoMoS(II)/C data (Table 3). Therefore, the conclusion is that the Co MoS(II) phase supported on carbon does not contain as much sulphur around Mo as the alumina or silica supported CoMoS(II) phases. With respect to the Mo–S coordination distance, no differences are observed between the samples studied, its value being 2.41 ± 0.005 Å, as in bulk MoS_2.

The Mo–Mo coordination number in Mo/Al (3.2) is significantly larger than that in CoMoS(I)/Al (2.8). This suggests that the presence of Co atoms indeed has an effect on the average MoS_2 slab dimension. Model calculations (using the Mo–Mo coordination numbers and assuming that the MoS_2 slabs are approximately round, flat discs) show that in Mo/Al on the average six or seven Mo atoms are present in the MoS_2 slab, and in CoMoS(I)/Al on the average five Mo atoms (in the heptamolybdate precursor of both samples, seven Mo atoms are clustered). According to Ledoux *et al.* (39), the role of Co in sulphided Co–Mo catalysts is to increase the fraction of Mo edge atoms. Thus this idea seems to be corroborated by the present EXAFS data showing that the average MoS_2 slab becomes smaller in CoMoS(I)/Al. However, for these small slab dimensions virtually all Mo atoms occupy edge positions, so this finding does not give positive proof for the idea proposed by Ledoux *et al.* (39).

In the alumina- and silica-supported CoMoS(II) catalysts, the Mo–Mo coordination numbers tend to be slightly larger than that in alumina-supported CoMoS(I): 3.1–3.4 vs, 2.8 (see Table 3). These findings suggest that the average dimension of the MoS_2 slabs in the alumina- and silica-supported CoMoS type II catalysts is larger than that in CoMoS(I)/Al: according to the model calculations, a Mo–Mo coordination number of 3.4 represents MoS_2 slabs with an average of seven Mo atoms. Also, the fact that the Debye–Waller factors for the Mo–Mo coordination shell (as for the Mo–S coordination shell) in the type II CoMoS samples are generally smaller than that for CoMoS(I)/Al suggests that the type II phase is better ordered, i.e., may consist of multilayers. This is in agreement with the very small CoMo(NTA)–support interaction (5), which provides very little means to effectively counteract any tendency of the MoS_2 particles to grow (fortunately small), while Mo is firmly fixed to the alumina surface in the CoMoS(I)/Al catalyst (40). At first,

it may seem unlikely that stacks of such small MoS_2 slabs are stable. However, in the most extreme case of CoMo S(II)/Al(0.32) the height/diameter ratio of the stacks is between 3/1 and 3/2; also the stacks may be more pyramidally than pillar-like in shape, EXAFS can not discern between those possibilities.

It is very remarkable that for the CoMoS(II)/C catalyst a Mo–Mo coordination number of only 2.3 is obtained, which indicates that the average MoS_2 slab size in this catalyst is even smaller than in CoMoS(I)/Al (on the average three or four Mo atoms). Also for the NiMoS(II)/C sample (similar to (16)) a low Mo–Mo coordination number was found (2.9). Remembering that the Mo–S coordination number for CoMoS(II)/C is also low, one wonders whether there is not a rather strong MoS_2–carbon support interaction, after all. In the case of graphite, evidence for such a strong sulphide–support interaction has been published (41). On the other hand, in our previous studies on Mo/C, involving dynamic oxygen chemisorption, thiophene HDS, and temperature-programmed sulphidation, such an interaction was not in evidence (42, 43). It may be, therefore, that agglomeration and stacking is prevented through physical trapping of the MoS_2 particles in the micropores of the carbon support. All this means that the origin of the monolayer type dispersion of the CoMoS(II)/C sample is still not understood. No change is observed for the Mo–Mo distance in the various samples studied, its value being 3.15 ± 0.01 Å as in bulk MoS_2.

A clear Mo–Co coordination could be observed in all catalyst samples at a distance varying from 2.77 to 2.84 Å, which is slightly lower than the Co–Mo distances obtained from the Co EXAFS data. However, the trend that in CoMoS(I)/Al andCoMoS(II)/C the Mo–Co distance is significantly smaller than in the other type II CoMoS samples (see Table 3), is also seen in the Co EXAFS data (Table 2). This may be connected with the monolayer arrangement in CoMoS(I)/Al and CoMoS(II)/C: the nearby support can induce changes in the Mo–Co interactions (vide infra).

Structure around Co in Type I and Type II CoMoS Phases

Co XANES results. Co in Co_9S_8 is mainly tetrahedrally surrounded by S, i.e., in sites lacking a centre of symmetry that cause a high intensity of the pre-edge peak. In all catalyst samples, the pre-edge feature is weak. The best resolved feature is seen for CoMoS(I)/Al and CoMo S(II)/Al(0.39). Perhaps in these samples a small fraction of the Co atoms is tetrahedrally surrounded, but it is also possible that there are Co atoms at square-pyramidal sites. Since we have no XANES data on a Co reference compound in which (most of) the Co atoms do occupy such a site, it is difficult to guess what fraction of Co atoms in CoMoS(I)/Al would occupy a square-pyramidal site, especially if this site is distorted to be intermediate between square-flat and square-pyramidal symmetry. The presence of the pre-edge feature in CoMoS(II)/Al(0.39) suggests that this sample may be intermediate between type I and type II CoMoS, although this would not have been concluded from the Mo-S coordination data, but it is corroborated by the fact that its catalytic activity is lower than that of CoMoS(II)/Al(0.32). Surprisingly, only a very faint pre-edge peak has been found for CoMoS(II)/C, which points to a more octahedrally or trigonal prismatic type of coordination. The absence of the pre-edge peak is not connected with the presence of a monolayer structure, since the intensity of the pre-edge feature is highest for CoMoS(I)/Al, which also has a monolayer type of dispersion.

Co EXAFS characteristics. The number of sulphur neighbouring atoms of Co increases from 4.9 to 6.3 in the order CoMoS(I)/Al < CoMoS(II)/Al(0.39) < CoMoS(II)/Si, CoMoS(II)/Al(0.32) < CoMoS(II)/C. The same trend is observed in the S/(Co + Mo) atomic ratios determined by XPS (Table 1), which shows a slightly higher value for CoMoS(II)/Al(0.32) (1.5 mol/mol) than for CoMoS(I)/Al (1.4 mol/mol) and a much higher value for CoMoS(II)/C (2.1 mol/mol). It can be concluded, therefore, that the Co atoms in type II CoMoS have a higher sulphur coordination than those in CoMoS(I)/Al. The Co–S coordination number for the CoMoS(II)/Al(0.39) catalyst lies between those of CoMoS(I)/Al and CoMoS(II)/Al(0.32), again indicating that this sample represents an intermediate between type I and type II CoMoS phases, as had already been concluded from the Co XANES results. The lowest and highest Co–S coordination numbers that have been encountered, also do fit nicely with the Co XANES results: for CoMoS(I)/Al, XANES hints that fivefold square-pyramidal symmetry may be present, in accordance with $N_{Co-S} = 4.9$; for CoMoS(II)/C, XANES agrees with (sixfold) octahedral or trigonal-prismatic arrangement, in accordance with $N_{Co-S} = 6.3$.

Besides the differences in coordination number, the alumina-supported catalysts show substantial differences in the Debye–Waller factor of the Co–S coordination: CoMoS(II)/Al(0.32), CoMoS(II)/Si < CoMoS(II)/Al(0.39) < CoMoS(I)/Al < CoMoS(II)/C. It appears that in CoMoS(II)/Al(0.32) and CoMoS(II)/Si this Debye–Waller factor is even negative with respect to the CoS_2 reference compound. It follows that in CoMoS(II)/Al(0.32) and CoMoS(II)/Si the disorder of the sulphur atoms is the smallest, suggesting the CoMoS phase present in these catalysts to be uniform and highly ordered. In contrast, the Debye–Waller factors for the Co–S shell

in CoMoS(I)/Al and especially in CoMoS(II)/C are much larger. The fact that in these samples MoS_2 is present in a monolayer arrangement, and thus all Co atoms must be near the support, may account for the observed differences. It must be kept in mind that the influence of the support is not exclusively that of bonding; just by its presence it may form a geometrical barrier for an undistorted arrangement of S atoms around Co. Again, CoMoS(II)/Al(0.39) is intermediate between CoMoS(I)/Al and CoMoS(II)/Al(0.32), strongly suggesting that in this sample stacking of the MoS_2 slabs has not taken place to the same extent as in the sample CoMoS(II)/Al(0.32).

In all our catalysts a Co–Mo coordination shell has been observed with interatomic distances ranging from 2.80 to 2.89 Å, duplicating the trend already observed in the Mo EXAFS results: the smallest distances are found for CoMoS(I)/Al and CoMoS(II)/C. The clear detection of this coordination shell in all samples is remarkable in view of its elusiveness in previous studies (cf. Introduction). It is, in our opinion, due to the fact that we have been able to prepare catalysts that contain only a single sulphided phase (cf. Experimental). Also, previous studies have mainly focused on conventionally prepared catalysts, containing mainly the CoMoS type I phase, which has indeed the smallest Co–Mo contribution. The ideas about the observed variation in the Debye–Waller factors of the Co–S shell (vide supra) also apply for the Co–Mo coordination distance: apparently the nearby support has a distorting influence on the environment of the Co atoms. On this interpretation, forcing the Co-atoms out of position in CoMoS(I)/Al and CoMoS(II)/C results in larger disorder in the Co–S shell and a shorter Co–Mo distance. The Co–Mo coordination numbers range from 0.9 to 1.9. In (15, 17, 44) it has been argued that the most likely position for the Co atoms is in front of the square sulphur faces of the MoS_6 trigonal prisms along the edges of the MoS_2 crystallites. On the basis of this model one would expect the Co–Mo coordination number to be close to 2.0. However, this value is only found for the CoMoS(II)/C sample. All other Co–Mo coordination numbers determined are much lower, within the limits of accuracy even 1.0 for CoMoS(I)/Al. This may be due to a large spread in Co–Mo coordination distances, resulting in an apparently lower Co–Mo coordination number, but it is also possible that subtle differences in Co coordination environment can be deduced from the differences in Co–Mo coordination number, a possibility that will be explored below.

Structural Model

Arrangement of the MoS_2 slabs. XPS, and EXAFS data in a more indirect way, fully agree with CoMoS(I)/Al having MoS_2 present in a monolayer arrangement. Opposed to that, it had been expected that the samples prepared via the NTA route would have MoS_2 present as multistacks. The multistack arrangement has been confirmed by XPS for CoMoS(II)/Al(0.32) (approx. five MoS_2 slabs stacked). It can also be concluded that CoMoS(II)/Si is very similar to its alumina-supported counterpart. The other two samples prepared according to the NTA route, deviate more or less. For CoMoS(II)/Al(0.39), especially the Co-edge data indicate that this sample is intermediate between CoMoS(I)/Al and CoMoS(II)/Al(0.32): it may be that in this sample the stacks are not as high as in CoMoS(II)/Al(0.32), or that a larger part of the MoS_2 slabs is present as a monolayer. For CoMoS(II)/C it is clear that stacking has not occurred. This follows directly from the XPS measurement and is corroborated by the fact that in many EXAFS and XANES features it is very similar to CoMoS(I)/Al.

Definition of the Co site. Co–S coordination numbers indicate that in the samples studied, both fivefold and sixfold Co–S coordinates occur. It may be concluded that in CoMoS(I)/Al, the coordination is almost exclusively fivefold (probably distorted square-pyramidal), while in CoMoS(II)/C the coordination is almost exclusively sixfold (probably distorted trigonal-prismatic). In the other CoMoS(II) samples a mixture of these two seems to be present, CoMoS(II)/Al(0.39) being close to CoMoS(I)/Al.

Apart from the Co–S coordination number, also the Co–Mo (Mo–Co) coordination number could provide information about the Co site. From Table 2, the extremes in Co-S coordination appear to be associated with a significant difference in Co-Mo coordination. For CoMoS(I)/Al a single coordination was found ($N_{Co-Mo} = 1.0$), while CoMoS(II)/C provides $N_{Co-Mo} = 1.9$, strongly suggesting a twofold coordination. This difference cannot be discerned in the Mo–Co coordination numbers, on first sight they seem to be very similar (see Table 3). However, one has to realize that (i) (different from the Co-edge) not all Mo atoms in the sample are coordinated to Co and (ii) Mo–Co EXAFS coordination numbers are averaged values if species with different type of Mo–Co coordinations are present. It is therefore possible to suggest a structural model in which CoMoS(II)/Al(0.39), CoMoS(II)/Si and CoMoS(II)/Al(0.32) can be thought to consist of a mixture of single and twofold Co–Mo coordinations: CoMoS(II)/Al(0.39) having the smallest fraction, and CoMoS(II)/Al(0.32) the largest fraction of twofold coordination. This is further explained in Appendix 1.

Structure of the CoMoS phase in the various samples. On the basis of the analyses described above, we propose (taking into account the limitations of our XPS and EXAFS data) that the CoMoS phase in the various samples can be described as follows (cf. Fig. 8):

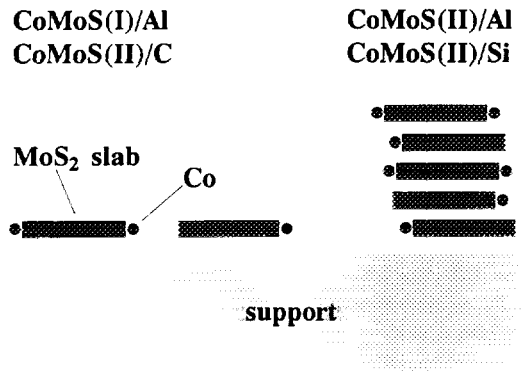

FIG. 8. Structural model of the CoMoS(I) and CoMoS(II) phases on different supports.

—in CoMoS(I)/Al the MoS_2 slabs are present as a monolayer, and the Co atoms are probably fivefold surrounded by S;

—in CoMoS(II)/Al(0.32) and CoMoS(II)/Si the MoS_2 slabs are stacked, and the Co–S coordination number is higher than in the previous case; part of the Co atoms may be surmised to be fivefold surrounded by S and to be attached to MoS_2 slabs on the support, like in Co MoS(I)/Al; the other part of the Co atoms would then be sixfold surrounded by S and be the ones attached to the MoS_2 slabs higher in the stacks;

—CoMoS(II)/Al(0.39) is intermediate in structure between CoMoS(I)/Al and CoMoS(II)/Al(0.32). A larger fraction of the MoS_2 slabs is in contact with the support than in CoMoS(II)/Al(0.32), hence a larger fraction of the Co atoms in the sample is probably fivefold surrounded by S;

—in CoMoS(II)/C the MoS_2 slabs are present in a monolayer dispersion, as in CoMoS(I)/Al, but here the Co atoms are probably sixfold surrounded by S.

In addition, a model is suggested in which the various phases can be further distinguished in terms of their Co–Mo coordination number: Co atoms attached to MoS_2 slabs in contact with SiO_2 or alumina then being singly coordinated to Mo, and Co atoms attached to MoS_2 slabs in contact with C or MoS_2 itself, being twofold coordinated to Mo. However, a Co site with a Co–Mo coordination number of 1 is not easy to envisage (44); more work is needed to conclusively establish this point.

Catalytic Characteristics of the Various CoMoS Phases

It is now worthwhile to try to relate the increase in specific HDS activity upon going from CoMoS type I or type II in the $CoMoS/Al_2O_3$ system to change in particle morphology, viz., single slabs in the type I phase and multilayer particles in the type II phase. It is possible that a multislab structure offers a (much) better accessibility of the reactants to the active sites, although in another context such an assumption did not obtrude itself (45). On the other hand, the EXAFS results show an increase of the Mo–S, Co–S, and Co–Mo coordination numbers as well as an increase in the structural ordering of the CoMoS particles in the type II phase with respect to those in the type I phase. The increased HDS activity is possibly related to one of these parameters.

To start and eliminate some of the possibilities, it is instructive to compare the EXAFS and XPS results of the CoMoS(II)/C catalyst, which has by far the highest specific HDS activity, with those of its alumina-supported counterparts. From the XPS data it is apparent that the MoS_2 phase in this catalyst is present as a monolayer. Thus, it follows that a multi-slab structure is not a prerequisite for a high specific thiophene HDS activity. The Mo-S coordination number and the structural disorder in CoMoS(II)/C are much more reminiscent of those characteristic of CoMoS(I)/Al than of those obtaining for the other CoMoS(II) catalysts. So, these parameters would not appear to provide a clue either. However, the Co–S and Co–Mo coordination numbers of CoMoS(II)/C deviate strongly, in being much higher than those of the other materials. This suggests that the thiophene HDS activity may correlate with the number of sulphur and perhaps molybdenum atoms in the first coordination shell of Co. Figure 9 shows a rather satisfactory relation between the Co–S coordination number and the thiophene activity. It may seem strange, on first sight, that catalytic activity should be found to increase with increasing Co–S coordination number, since one needs vacant coordination sites to adsorb the reactant(s), but we need to remember that the EXAFS spectra are taken at low temperature after a purging procedure that leaves quite a substantial amount

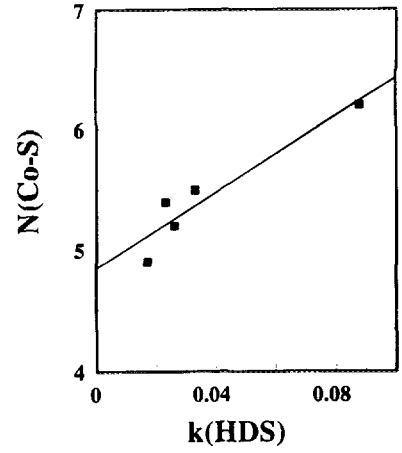

FIG. 9. Specific thiophene HDS activity (per mol Co present) as a function of the Co–S coordination number for the sulfided CoMo samples.

of adsorbed sulphur species on the active phase (46). It is of course satisfying to find that it is the local structure of the Co atoms that is related to the HDS activity, since Topsøe has shown that the activity of CoMo/Al catalysts is linearly related to the amount of Co in CoMoS. Moreover, our previous work has provided evidence that the Co sites can be considered to constitute the active HDS sites (3).

If the HDS of thiophene takes place via direct hydrogenolysis, the relationship depicted in Fig. 9 can be understood relatively easily: it is the left hand side of a volcano plot relating the HDS activity to the sulphur adsorption strength (taking the observed Co–S coordination number to consist of a fixed, stoichiometric, and a variable, adsorbed part), where the hydrogenolysis step is rate-determining. The right-hand side, where the hydrogenation of the adsorbed sulphur is rate determining, is apparently not (yet) accessible in the CoMo system. However, it remains unclear why the Co–S and Co–Mo coordination numbers of the different Co-sites vary in the way they appear to do.

CONCLUSIONS

The main conclusions from the present work are as follows:

—In all catalysts employed in the present study a CoMoS phase is the only sulphided phase present. Both a Co–Mo and a Mo–Co coordination shell can be detected, proving that in the CoMoS phase the Co atoms are positioned on the outside of the MoS_2 particles, in the same plane as the Mo atoms.

—The CoMoS type II phase supported on alumina is present as a multilayer structure, whereas the type I phase exists as a single-slab, i.e., monolayer, structure.

—The silica-supported CoMoS type II phase closely resembles its alumina-supported counterpart. The carbon-supported CoMoS type II phase, on the other hand, shows a Mo–S coordination number, structural ordering, and degree of stacking much more similar to CoMoS(I)/Al. It is therefore questionable whether the designation "type II," as being a fully sulphided and not chemically bonded phase to the support, is really appropriate. The most characteristic features of CoMoS(II)/C are its very high Co–S and Co–Mo coordination numbers and the high degree of structural disorder of the sulphur atoms surrounding Co.

—In the suite of catalysts studied here, two types of Co-sites could be discerned. One consists of a single Co–Mo coordination, which is the predominant site in the least-active CoMoS(I)/Al and CoMoS(II)/Al(0.39) samples. The other one has an approximately sixfold Co–S coordination and possibly a twofold Co–Mo coordination, which constitutes a large part of the Co-sites in CoMoS(II)/Si and CoMoS(II)/Al(0.32), and seems to be the exclusive site in CoMoS(II)/C. From the catalytic activities of the samples, it is clear that the latter type of site is the most active. Thus a correlation has been found between the specific (i.e., per mol Co) thiophene HDS activity and the Co–S coordination number, as determined in freshly sulphided, purged, and cooled samples. A high number of sulphur neighbours appears to correlate with a high specific HDS activity.

APPENDIX 1

An attempt has been made to determine the Mo-environment of the Co atoms in the CoMoS phases using both the EXAFS Co–Mo and Mo–Co coordination numbers, on the assumption that the observed differences in the latter do indeed correlate with real differences in CoMoS structure.

For a catalyst sample similar to the suite of CoMoS samples studied here, with 6 Mo atoms per slab on the average, and Co/Mo = 0.33 (at/at), the average slab can be visualized as follows:

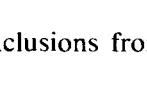

○ = Co atom, N(Co–Mo) = 1,
● = Co atom, N(Co–Mo) = 2,
X = Mo atom in MoS_2.

(The fraction of Co atoms with N(Co–Mo) = 1 is arbitrary; the fact that Co atoms with N(Co–Mo) = 1 should perhaps occur in pairs is not taken into account now.)

From the Co–Mo coordination number is easy to determine the fraction x of twofold (by Mo) coordinated Co atoms:

—twofold: N(Co–Mo) = 2;
—single: N(Co–Mo) = 1;
—$N(\text{Co–Mo})_{exp} = 2x + 1(1 - x)$, from which follows the fraction x.

From the Mo–Co coordination number it is more difficult to see how the fraction x should be determined. As can be seen in the drawing above, with a typical Co/Mo ratio of 0.33 not all Mo atoms in the MoS_2 slab have Co atoms in their immediate environment, and the Mo–Co coordination number determined from EXAFS thus also reflects the Co/Mo atomic ratio:

—twofold: $N(\text{Mo–Co}) = 2(\text{Co/Mo}_{exp})$;
—single: $N(\text{Mo–Co}) = \text{Co/Mo}_{exp}$;
—$N(\text{Mo–Co})_{exp} = 2(\text{Co/Mo}_{exp})x + (\text{Co/Mo}_{exp})(1 - x)$, from which also follows the fraction x.

In the ideal case, the numerical values for the fractions x derived from N(Co–Mo) and N(Mo–Co) should coincide. Below, we compare the calculations for all samples. The experimental coordination numbers for the Co–Mo and

Mo–Co shells are taken from Table 2 and Table 3, respectively:

Sample	Co/Mo	Shell	N	Fraction	Twofold
CoMoS(I)/Al	0.56	Co–Mo	1.0 ± 0.3	0	(<0.3)
		Mo–Co	0.6 ± 0.2	0.1	(<0.5)
CoMoS(II)/Al	0.39	Co–Mo	0.9 ± 0.4	0	(<0.3)
		Mo–Co	0.6 ± 0.2	0.5	(>0.1)
CoMoS(II)/Si	0.30	Co–Mo	1.4 ± 0.3	0.4	(0.1–0.7)
		Mo–Co	0.6 ± 0.2	1	(>0.3)
CoMoS(II)/Al	0.32	Co–Mo	1.5 ± 0.3	0.5	(0.2–0.8)
		Mo–Co	0.6 ± 0.2	0.9	(>0.3)
CoMoS(II)/C	0.32	Co–Mo	1.9 ± 0.5	0.9	(>0.4)
		Mo–Co	0.7 ± 0.3	1	(>0.3)

From this table it can be seen from the two extremes of the series, CoMoS(I)/Al and CoMoS(II)/C, the fractions determined from the Co–Mo and the Mo–Co coordination numbers do coincide very closely, whereas for the other samples the gaps are larger, but still within the reliability range. Although coincidence is not perfect, we think that in view of the difficult extraction of the Co–Mo and Mo–Co references from the EXAFS of the Ni–Mo cluster compound (see Experimental section), the agreement of the results derived from the Co–Mo and Mo–Co coordination shells may be considered to be satisfactory. As a final value for the fraction of twofold coordinated Co (by Mo) we have therefore taken the mean value of those calculated on the basis of the Co–Mo and Mo–Co coordination numbers for each sample:

Sample	Fraction twofold
CoMoS(I)/Al	0
CoMoS(II)/Al(0.39)	0.2
CoMoS(II)/Si	0.7
CoMoS(II)/Al(0.32)	0.7
CoMoS(II)/C	1

REFERENCES

1. Topsøe, H., Clausen, B. S., Topsøe, N., and Pedersen, E., *Ind. Eng. Chem. Fundam.* **25,** 25 (1986); Topsøe, H., and Clausen, B. S., *Appl. Catal.* **25,** 273 (1986).
2. Topsøe, H., Clausen, B. S., Candia, R., Wivel, C., and Morup, S., *J. Catal.* **68,** 433 (1981); Wivel, C., Candia, R., Clausen, B. S., Morup, S., and Topsøe, H., *J. Catal.* **68,** 453 (1981).
3. Prins, R., de Beer, V. H. J., and Somorjai, G. A., *Catal. Rev. - Sci. Eng.* **31,** 1 (1989).
4. Candia, R., Sorensen, O., Villadsen J., Topsøe, N., Clausen, B. S., and Topsøe, H., *Bull. Soc. Chim. Belg.* **93,** 763 (1984).
5. van Veen, J. A. R., Gerkema, E., van der Kraan, A. M., and Knoester, A., *J. Chem. Soc. Chem. Commun.*, 1684 (1987).
6. van Veen, J. A. R., Gerkema, E., van der Kraan, A. M., Hendriks, P. A. J. M., and Beens, H., *J. Catal.* **133,** 112 (1992).
7. van der Kraan, A. M., Crajé, M. W. J., Gerkema, E., Ramselaar, W. L. T. M., and de Beer, V. H. J., *Appl. Catal.* **39,** L7 (1988); Crajé, M. W. J., de Beer, V. H. J., and van der Kraan, A. M., *Appl. Catal.* **70,** L7 (1990).
8. Topsøe, N., and Topsøe, H., *J. Catal.* **84,** 386 (1983); these observations could be reproduced by us: Fierro, J. L. G., and van Veen, J. A. R., unpublished.
9. Clausen, B. S., Lengeler, B., Candia, R., Als-Nielsen, J., and Topsøe, H., *Bull. Soc. Chim. Belg.* **90,** 1249 (1981); Clausen, B. S., Topsøe, H., Candia, R., Villadsen, J., Lengeler, B., Als-Nielsen, J., and Christensen, F., *J. Phys. Chem.* **85,** 3868 (1981).
10. Bommannavar, A. S., and Montano, P. A., *Appl. Surf. Sci.* **19,** 250 (1984).
11. Sankar, G., Vasudevan, S., and Rao, C. N. R., *J. Phys. Chem.* **91,** 2011 (1987).
12. Parham, T. G., and Merrill, R. P., *J. Catal.* **85,** 295 (1984).
13. Clausen, B. S., and Topsøe, H., *Hyperfine Int.* **47,** 203 (1989).
14. Bauer, S. H., Chiu, N.-S., and Johnson, M. F. L., *J. Phys. Chem.* **90,** 4888 (1986).
15. Niemann, W., Clausen, B. S., and Topsøe, H., *Catal. Lett.* **4,** 355 (1990).
16. Bouwens, S. M. A. M., Koningsberger, D. C., de Beer, V. H. J., Louwers, S. P. A., and Prins, R., *Catal. Lett.* **5,** 273 (1990).
17. Bouwens, S. M. A. M., van Veen, J. A. R., Koningsberger, D. C., de Beer, V. H. J., and Prins, R., *J. Phys. Chem.* **95,** 123 (1991); Crajé, M. W. J., Ph.D. Thesis, Univ. Delft, The Netherlands, 1992.
18. Konings, A. J. A., van Doorn, A. M., Koningsberger, D. C., de Beer, V. H. J., Farragher, A. L., and Schuit, G. C. A., *J. Catal.* **54,** 1 (1978).
19. Kuipers, H. P. C. E., *Solid State Ionics*, **16,** 15 (1985).
20. Kampers, F. W. H., Maas, T. M. J., van Grondelle, J., Brinkgreve, P., and Koningsberger, D. C., *Rev. Sci. Instrum.* **60,** 2635 (1989).
21. Cook, J. W., and Sayers, D. E., *J. Appl. Phys.* **52,** 5024 (1981).
22. van Zon, J. B. A. D., Koningsberger, D. C., van't Blik, H. F. J., and Sayers, D. E., *J. Chem. Phys.* **82,** 5742 (1985).
23. Teo, B.-K., and Lee, P. A., *J. Am Chem. Soc.* **10,** 2815 (1979).
24. Morris, B., Johnson, V., and Wold, A., *J. Phys. Chem. Solids* **28,** 1565 (1965).
25. Bouwens, S. M. A. M., Prins, R., de Beer, V. H. J., and Koningsberger, D. C., *J. Phys. Chem.* **94,** 3711 (1990); Bouwens, S. M. A. M., Ph. D. Thesis, Univ. Eindhoven, The Netherlands, 1988.
26. Sotofte, I., *Acta Chem. Scand.* **A30,** 57 (1976).
27. Lytle, F. W., Sayers, D. E., and Stern, E. A., *Physica B* **158,** 701 (1989).
28. Gurman, S. J., Binsted, N., and Ross, I., *J. Phys. C* **17,** 143 (1984).
29. van Dijk, M. P., van Veen, J. A. R., Bouwens, S. M. A. M., van Zon, F. B. M., and Koningsberger, D. C., *in* "Proc. 2nd Eur. Conf. Progr. X-Ray Synchr. Rad. Res." (A. Balerna *et al.*, Eds.), Vol. 25, p. 139. SIF, Bologna, 1990.
30. Vaarkamp, M., Dring, I., Oldman, R. J., Stern, E. A., and Koningsberger, D. C., submitted for publication.
31. Kampers, F. W. H., Ph.D. Thesis, Univ. Eindhoven, The Netherlands, 1988.
32. Alstrup, I., Chorkendorff, I., Candia, R., Clausen, B. S., and Topsøe, H., *J. Catal.* **77,** 397 (1982).
33. Bahl, O. P., Evans, E. L., and Thomas, J. M., *Proc. R. Soc. London Ser. A* **306,** 53 (1968).
34. Bouwens, S. M. A. M., Koningsberger, D. C., de Beer, V. H. J., and Prins, R., *Catal. Lett.* **1,** 55 (1988).
35. Shulman, R. G., Yafet, Y., Eisenberger, P., and Blumberg, W. E., *Proc. Natl. Acad. Sci. U.S.A.* **73,** 1384 (1976).
36. Kemp, R. A., Ryan, R. C., and Smegal, J. A., *in* "Proceedings, 9th International Congress on Catalysis, Calgary, 1988" (M. J. Phillips and M. Ternan, Eds.), Vol. 1, p. 128. The Chemical Inst. of Canada, Ottawa, 1988.
37. van Veen, J. A. R., Hendriks, P. A. J. M., Andrea, R. R., Romers, E. J. G. M., and Wilson, A. E., *J. Phys. Chem.* **94,** 5282 (1990);

Eijsbouts, S., van Gestel, J. N. M., van Veen, J. A. R., de Beer, V. H. J., and Prins, R., *J. Catal.* **131,** 412 (1991).
38. Boudart, M., Arrieta, J. S., and Dalla Betta, R., *J. Am. Chem. Soc.* **105,** 6501 (1982).
39. Ledoux, M. J., Maire, G., Hantzer, S., and Michaux, O., *in* "Proceedings, 9th International Congress on Catalysis, Calgary, 1988" (M. J. Phillips and M. Ternan, Eds.), Vol. 1, p. 74. The Chemical Inst. of Canada, Ottawa, 1988.
40. van Veen, J. A. R., Gosselink, J. W., Meuris, T., Reinalda, D., de Vries, A. F., and Stork, W. H. J., *in* "Proc. TOCAT 1," paper 113. 1990.
41. Hayden, T. F., Dumesic, J. A., Sherwood, R. D., and Baker, R. T. K., *J. Catal.* **105,** 299 (1987).
42. Vissers, J. P. R., Bachelier, J., ten Doeschate, H. J. M., Duchet, J. C., de Beer, V. H. J., and Prins, R., *in* "Proceedings, 8th International Congress on Catalysis, Berlin, 1984," Vol. 2, p. 387. Dechema, Frankfurt-am-Main, 1984.
43. Vissers, J. P. R., Scheffer, B., de Beer, V. H. J., Moulijn, J. A., and Prins, R., *J. Catal.* **105,** 277 (1987).
44. Topsøe, H., Clausen, B. S., Topsøe, N., and Zeuthen, P., *in* "Catalysts in Petroleum Refining 1989" (A. L. Trimm *et al.*, Eds.), p. 77. Elsevier, Amsterdam, 1990.
45. Gosselink, J. W., Schaper, H., de Jonge, J. P., and Stork, W. H. J., *Appl. Catal.* **32,** 337 (1987).
46. Mangnus, P. J., Ph.D. Thesis, Univ. Amsterdam, The Netherlands, 1991.